

# A Novel Miniaturized Tri-band VCO Utilizing a Three-mode Reconfigurable Inductor

Seongwoog Oh<sup>1</sup>, Jungsuek Oh<sup>2</sup>

Institute of New Media and Communications (INMC) and the Department of Electrical and Computer Engineering, Seoul National University, Seoul, South Korea

<sup>1</sup>dillon1859@snu.ac.kr, <sup>2</sup>jungsuek@snu.ac.kr

**Abstract**—A novel miniaturized tri-band complementary metal-oxide-semiconductor (CMOS) voltage-controlled oscillator (VCO) utilizing a three-mode reconfigurable inductor is proposed. The reconfigurable inductor consists of primary and secondary windings with a center loop connected to each winding center-tap to enable three-mode operation. By adjusting the diameter of each winding and loop, the equivalent inductance for each mode can be designed independently, resulting in a high degree of freedom for a tri-band VCO with minimal Q-factor degradation. The VCO implemented in a 28nm CMOS process shows frequency tuning ranges of 16.78 – 20.13GHz, 19.8 – 24.15GHz, and 33 – 41.13GHz for each mode with corresponding phase noise and tuning range figure-of-merit (FoM<sub>T</sub>) values of -190.1, -190.9, -194.6dBc/Hz. The fabricated chip consumes 12.72mW and occupies a core area of 0.043mm<sup>2</sup>.

**Keywords**—Inductive frequency tuning, millimeter wave circuits, reconfigurable inductor, tri-band, voltage-controlled oscillator

## I. INTRODUCTION

With the 5G era, the demand for transceivers at millimeter wave frequencies is steadily increasing. As frequency bandwidth requirements increase, millimeter-wave transceivers also must be guaranteed for multi-band operation [1]. For multi-band operation, different oscillators that generate each required frequency are needed, which is undesirable due to the increased chip area. Several topologies have been proposed for multi-band oscillators to avoid the aforementioned issue [2-7]. When using dividers and mixers combined with a single-band VCO, the frequency of each signal cannot be controlled independently. Multi-band implementation is possible by controlling the current path in the inductor or transmission line through switching. However, when the oscillation band is shifted, the total size of the inductive component increases to support various inductance configurations, and the Q-factor degrades due to switch resistance. In particular, the aforementioned issues start to affect the performance critically when the number of supporting band increases, and existing tri-band VCOs do not perform well on all bands.

In this work, a tri-band VCO operating on the K and Ka bands using a three-mode reconfigurable inductor is proposed. In order to combine the proposed inductor with the VCO with low loss levels, the effect of switch resistance on the LC tank is minimized and three oscillation cores are configured to implement the tri-band operation. Section II covers the operating and design procedure of the proposed inductor and

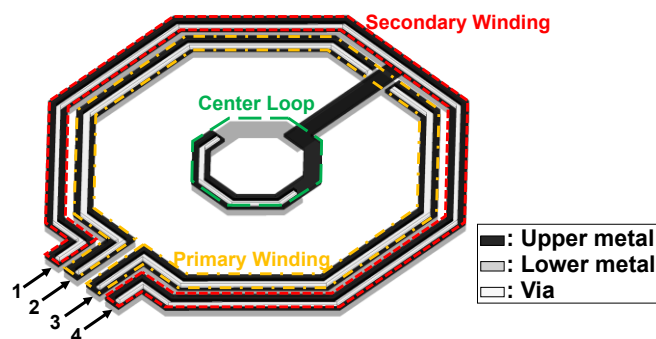


Fig. 1. Diagram of the proposed three-mode reconfigurable inductor.

VCO. Section III shows the fabricated VCO chip in a 28nm bulk-CMOS process with measurement results.

## II. THREE-MODE RECONFIGURABLE INDUCTOR

As shown in Fig. 1, a three-mode reconfigurable inductor with a diagram consisting of a primary winding, a secondary winding, and a center loop has been proposed. The primary and secondary windings use multiple thick metals throughout with vias provided by the process to minimize the ohmic loss due to resistance. Both ends of the center loop are connected to the center tap of each winding, and to prevent a short circuit, only the upper and lower metal is combined with the primary and secondary windings, respectively. Therefore, the proposed inductor consists of four ports, as both nodes of the primary and secondary windings are used as each port for reconfigurability.

Three-mode operation of the reconfigurable inductor is achieved by controlling the excitation of each port, as shown in Fig. 2. As shown in Fig. 2(a), when ports 1 and 3 are excited as positive and ports 2 and 4 are excited as negative, the input voltage of each winding is out of phase (odd mode). Because both winding nodes are excited in a differential mode, a virtual ground is formed at each center tap, meaning that no current flows through the center loop. Therefore, current flows only along each winding in the opposite direction, which results in negative mutual inductance. When the input voltage of each winding is in phase (even mode), the operation is similar to that in the odd mode, with the difference that the direction of current flowing through each winding is identical, meaning that the mutual inductance is positive, as shown in Fig. 2(b). Additionally, when ports 1 and 4 are positively excited and ports 2 and 3 are negatively excited, the center tap

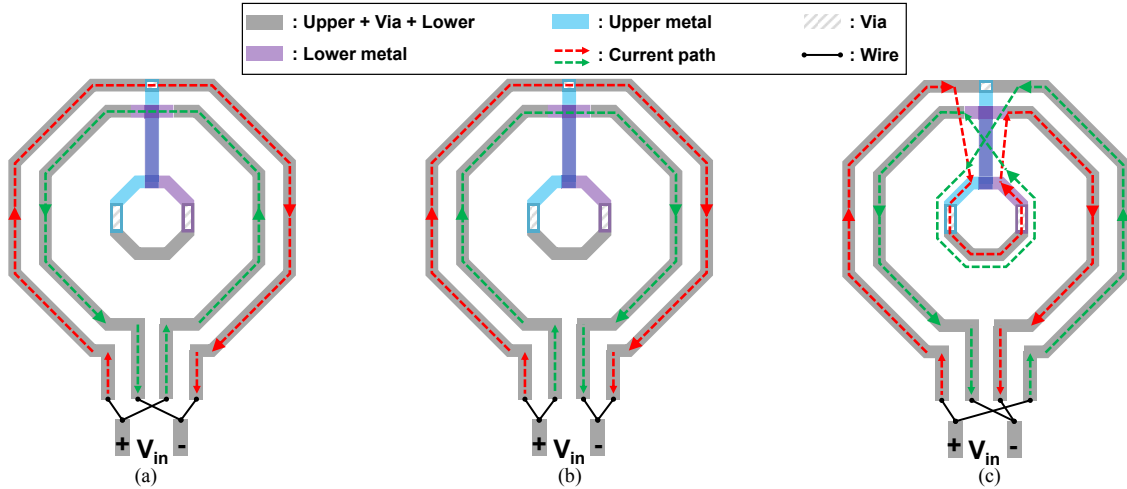


Fig. 2. Excited current paths according to the (a) odd, (b) even, and (c) expansion modes in the proposed inductor. Each red and green dashed arrow identifies the current path from the positive node to the negative node by the inductor port.

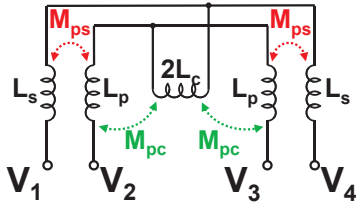


Fig. 3. Simplified equivalent circuit model of the proposed three-mode reconfigurable inductor.

is no longer a virtual ground (expansion mode). In Fig. 2(c), a potential difference is formed between each center tap, and current flows through the windings and the center loop.

Fig. 3 shows the equivalent circuit configuration of the proposed inductor. In the odd mode, because there is no center loop in the current path, the schematic consists only of  $L_p$  and  $L_s$ , correspondingly equal to half of the self-inductance of the primary and secondary windings, and the negative mutual inductance,  $M_{ps}$ , which is positive for the even mode. In the expansion mode, given that the center loop is added to the current path  $L_c$ , which is half of the self-inductance of the center loop, the mutual inductance with the primary winding,  $M_{pc}$ , must be considered. Therefore,  $L_p$ ,  $L_s$ , and  $M_{ps}$  are the main factors that directly determine the inductance in the odd and even mode,  $L_{odd}$  and  $L_{even}$ , respectively. The difference in  $L_{odd}$  and  $L_{even}$  is affected by  $M_{ps}$ , which can be adjusted by changing the spacing between the two windings. Inductance in the expansion mode is obtained by  $L_p$ ,  $L_s$ ,  $M_{ps}$  as well as the additional variables of  $L_c$  and  $M_{pc}$ . The mutual inductance between the secondary coil and the center loop,  $M_{sc}$ , is neglected due to its relatively small value compared to those of the other inductances due to the isolation effect caused by the primary winding.

Fig. 4(a) plots the simulated normalized inductance of each mode when the diameters of the secondary winding and center loop are fixed at  $150\ \mu\text{m}$  and  $50\ \mu\text{m}$ , respectively, and the diameter of the primary winding is increased from  $85\ \mu\text{m}$  to  $120\ \mu\text{m}$  with a width of  $10\ \mu\text{m}$ . The inductance variations in the odd and expansion modes are 26% and 19%, respectively,

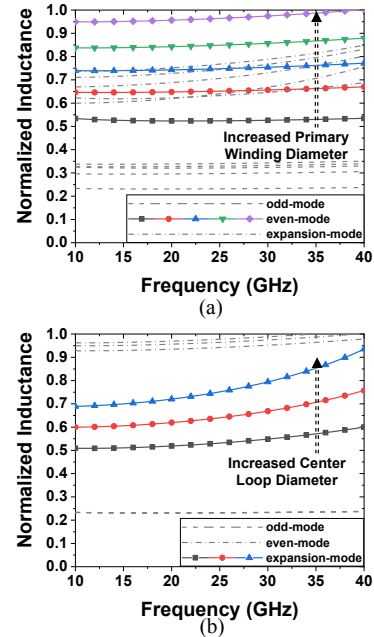


Fig. 4. Inductance for each mode of the proposed three-mode reconfigurable inductor with respect to the (a) primary winding and (b) the center loop diameter change.

while the change in the even mode is 59%. As the diameter increases, not only does  $L_p$  increase, but the absolute value of  $M_{pc}$  decreases, whereas the absolute value of  $M_{ps}$  increases. Fig. 4(b) shows the inductance for each mode when the diameter of the center loop is increased from  $40\ \mu\text{m}$  to  $60\ \mu\text{m}$  for fixed primary and secondary winding dimensions. Because current flows in the center loop only in the expansion mode, the inductance variations in the odd and even mode are 0.6% and 3.6%, respectively, both of which are negligible compared to the results in Fig. 4(a), while the variation is 33% for the expansion mode. To adjust the inductance value in each three-mode reconfigurable inductor, it is necessary to obtain the desired inductance for the odd and even mode by adjusting the diameters of the primary and secondary windings. Then, the

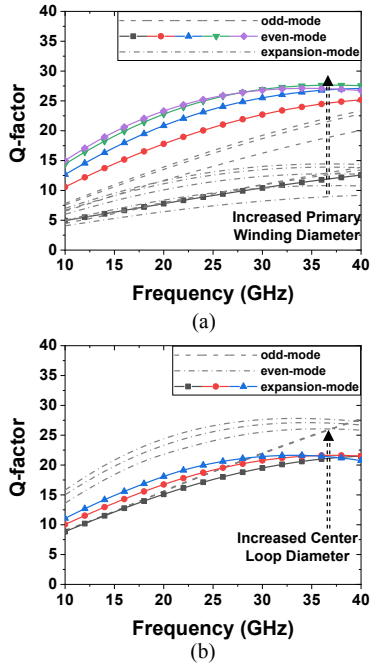


Fig. 5. Q-factor for each mode of the proposed three-mode reconfigurable inductor with respect to (a) the primary winding and (b) a change in the center loop diameter.

diameter of the center loop is optimized to complete the fine-tuning of the inductance in the expansion mode.

Fig. 5 plots the Q-factor, which changes in response to a change in the dimensions in Fig. 4. From Fig. 5(a), when the primary winding and the center loop are separated by more than a certain distance (primary winding diameter  $> 100 \mu\text{m}$ ), the q-factor varies within a value of 1 at 30 GHz or more. It can be seen that the effect on the expansion-mode q-factor during the change of the center loop dimension as well as the other modes is small.

A schematic of a tri-band VCO utilizing the proposed three-mode reconfigurable inductor is shown in Fig. 6. In total, three cores with a varactor connected to an inductor are connected to a simple cross-coupled pair to generate negative transconductance. A switch array is used for mode operation between the drain nodes of the transistor and the connected inductor nodes and enters the ON-state when high voltage is applied to the bit. Because the switch arrays used in this design are connected in parallel to the current flowing through the inductor, the voltage headroom is not affected and losses due to switch resistance are minimized.

For odd mode oscillation, the control bit of each switch must be applied in the following form:  $(SW_{odd}, SW_{even}, SW_{expansion}) = (\text{High}, \text{Low}, \text{Low})$ . At the same time,  $V_{g1}$  and  $V_{g3}$  must be high enough so that the corresponding oscillation core compensates for the loss of the LC tank, while  $V_{g2}$  should be below the threshold voltage to ensure that core2 turns off. For even mode operation, the core voltage must be applied with the same configuration as the odd mode, and the control bit for the switch array is set as follows:  $(SW_{odd}, SW_{even}, SW_{expansion}) = (\text{Low}, \text{High}, \text{Low})$ . However, for expansion mode operation,  $V_{g1}$  and  $V_{g3}$  should be below the threshold voltage and  $V_{g2}$

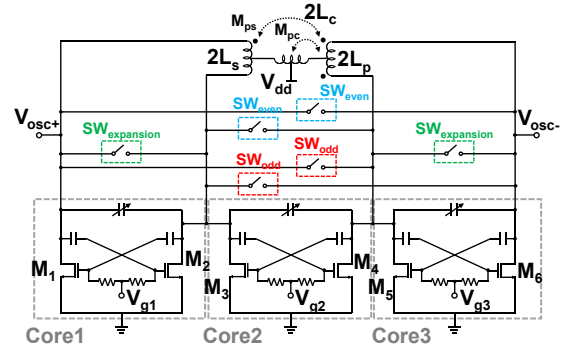


Fig. 6. Schematic of the proposed VCO with three cores and a switch array. The proposed three-mode reconfigurable is utilized to enable tri-band operation.

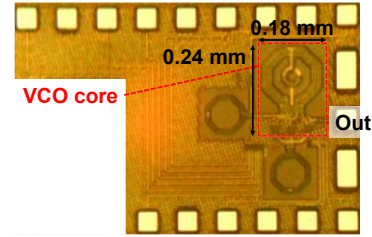


Fig. 7. Die photograph of the proposed tri-band VCO.

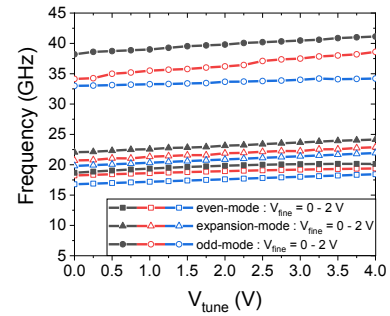


Fig. 8. Measured frequency tuning for even, expansion, and odd mode operation

must be high enough for oscillation with the  $(SW_{odd}, SW_{even}, SW_{expansion}) = (\text{Low}, \text{Low}, \text{High})$  control bit applied. Given that the expansion mode operates using a single core, the width of the transistor  $M_{3-4}$  is 1.8 times that of  $M_{1-2}$  and  $M_{5-6}$  to make it similar to the negative transconductance of the odd and even modes.

### III. IMPLEMENTATION AND MEASUREMENT RESULTS

The proposed tri-band VCO is fabricated in the Samsung 28nm bulk-CMOS process with a core size of  $0.18 \text{ mm} \times 0.24 \text{ mm}$  (Fig. 7). From a 1.2V supply, the VCO core consumes 10.6 – 21 mW depending on the operation mode for band reconfiguration.

The measured frequency tuning range is shown in Fig. 8 when operating in each mode with tuning voltage applied from 0 – 4 V to ensure not to exceed the breakdown voltage centered on 2 V. The operation of each oscillation core is determined according to the operation of each mode. The voltage controlling the varactor of the turned-on core is  $V_{tune}$ , and the voltage controlling the varactor of the turned-off core is  $V_{fine}$ . By combining coarse ( $V_{tune}$ ) and fine ( $V_{fine}$ ) tuning of

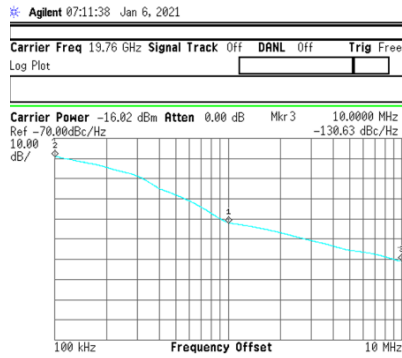


Fig. 9. Measured phase noise for even-, expansion-, and odd-mode operation.

the varactor, the measured frequency ranges are from 16.78GHz to 20.13GHz when the even mode is selected, 33GHz to 41.13GHz when the odd mode is selected, and 19.8GHz to 24.15GHz when the expansion mode is selected.

The measured phase noise for proposed VCO is plotted in Fig. 9. The phase noise measured in the even mode (19.8GHz) is -130.6dBc/Hz at 10-MHz offsets. The phase noise is lowest in the even mode; these values are 1.4dB and 3.1dB higher for the odd mode and expansion mode, respectively. The observation of the phase noise performance for each mode is consistent with the simulated q-factor result of the proposed three-mode reconfigurable inductor.

Table 1 compares the performance capabilities of the fabricated VCO with other dual-band and tri-band VCOs. For comparison, the phase noise figure-of-merit (FoM) and FoM<sub>T</sub> with phase noise and a frequency tuning range (FTR) are used. The proposed tri-band VCO achieves excellent FoM and FoM<sub>T</sub> outcomes for all modes in a small area. To the best of the authors' knowledge, this VCO achieves the lowest average FoM<sub>T</sub> in silicon on the K and Ka bands with triple-mode operation.

#### IV. CONCLUSION

A miniaturized tri-band VCO with a three-mode reconfigurable inductor is proposed in this paper. The tri-band VCO operating on the K band and the Ka band and occupying an area of 0.043 mm<sup>2</sup> is fabricated using a 28nm bulk-CMOS process. The proposed inductor can independently adjust the

equivalent inductance obtained in each mode. The measured VCO achieved a FoM<sub>T</sub> level of -190dBc/Hz or less at the frequencies of 18.46GHz, 21.98GHz, and 37.07GHz.

#### ACKNOWLEDGMENT

This work was supported by Institute of Information & communications Technology Planning & Evaluation (IITP) grant funded by the Korea government (MSIT) (No.2020-0-00858, Millimeter-wave Metasurface-based Dual-band Beamforming Antenna-on-Package Technology for 5G Smartphone) and Samsung Electronics (Development of Dual-band/Wide-band High Efficiency Power Amplifier MMIC for 5G Applications). The chip fabrication and EDA tool were supported by the IC Design Education Center (IDEC), Korea.

#### REFERENCES

- [1] Z. Pi and F. Khan, "An introduction to millimeter-wave mobile broadband systems," *IEEE Communications Magazine*, vol. 49, no. 6, pp. 101–107, Jun. 2011.
- [2] Y. Chen, Y. Pei, D. and M. W. Leenaerts, "A dual-band LO generation system using a 40GHz VCO with a phase noise of -106.8dBc/Hz at 1-MHz," *IEEE Radio Frequency Integrated Circuits Symposium*, pp. 203–206, Jun. 2013.
- [3] L. Wu, A. W. L. Ng, L. L. K. Leung, and H. C. Luong, "A 24-GHz and 60-GHz Dual-band Standing-wave VCO in 0.13- $\mu$ m CMOS process," in *IEEE Radio Frequency Integrated Circuits Symposium*, pp.145–148, Jun. 2010.
- [4] Y. Itoh, W. Xiaole, S. Omokawa, "A Triple-Band SiGe HBT Cross-Coupled Differential VCO Using a Novel Element-Switching Technique," *2018 Asia-Pacific Microwave Conference (APMC)*, pp. 255–257, Nov. 2018.
- [5] J. Baylon, P. Agarwal, L. Renaud, S. N. Ali, and D. Heo, "A Ka-Band Dual-Band Digitally Controlled Oscillator With -195.1-dBc/Hz FoM<sub>T</sub> Based on a Compact High-Q Dual-Path Phase-Switched Inductor," *IEEE Transactions on Microwave Theory and Techniques*, vol. 67, no.7, pp.2748–2758, Jul. 2019.
- [6] S.-L. Liu, K.-H. Chen, and A. Chin, "A dual-resonant mode 10/22-GHz VCO with a novel inductive switching approach," *IEEE Transactions on Microwave Theory and Techniques*, vol. 60, no. 7, pp. 2165–2177, Jul. 2012.
- [7] S. Jain and S. Jang, "Triple-Band Transformer-Coupled LC Oscillator With Large Output Voltage Swing," *IEEE Microwave and Wireless Components Letters*, vol. 24, no. 7, pp. 475–477, Jul. 2014.
- [8] D. Cabrera, J. B. Begueret, N. Verrascina, O. Tesson, O. Mazouffre, and P. Gamand, "A low phase noise tri-band LO generation for Ku and E band radios for backhauling Point-to-Point applications," *IEEE Bipolar/BiCMOS Circuits and Technology Meeting*, pp. 56–59, Sep. 2016.

Table 1. Performance Comparison of Tri-band VCOs

	This work	[5]	[6]	[7]	[8]
Type	Tri-band VCO	Dual-band VCO	Dual-band VCO	Tri-band VCO	Tri-band VCO
Technology	28nm CMOS	65nm CMOS	180nm CMOS	180nm CMOS	0.25 $\mu$ m SiGe:C
Freq. (GHz)	18.46/21.98/37.07	16.75/23.7	10.7/22	3.49/7.53/8.51	18/36/67
FTR (%)	18.2/19.8/21.9	23.3/24.4	7.6/8	24.2/2.91/6.35	9.5
PN <sub>norm</sub> (dBc/Hz)	-195.9/-196/-198.9	-192.5/-194.1	-196.5/-193.6	-193.9/-197.1/-196.9	-198.4/-198.8/-196.5
P <sub>DC</sub> (mW)	12.72	4.8	15.2	3.3/4/4.2	95
FoM (dBc/Hz)	-184.9/-185/-187.8	-185.7/-187.2	-184.7/-181.8	-188.7/-191.1/-190.7	-178.6/-179.1/-176.7
FoM <sub>T</sub> (dBc/Hz)	-190.1/-190.9/-194.6	-193/-195	-182.2/-179.9	-196.4/-180.4/-186.8	-178.1/-178.6/-176.3
Size (mm <sup>2</sup> )	0.043	0.046	0.75	0.57	0.329

$$PN_{\text{norm}} = L\{\Delta f\} - 20\log\left(\frac{f_{\text{osc}}}{\Delta f}\right);$$

$$FoM_{\text{PN}} = L\{\Delta f\} - 20\log\left(\frac{f_{\text{osc}}}{\Delta f}\right);$$

$$FoM_{\text{T}} = FoM_{\text{PN}} - 20\log(10 \cdot FTR)$$